Ewald Summation Versus Direct Summation of Shifted-Force Potentials for the Calculation of Electrostatic Interactions in Solids: A Quantitative Study

H. DUFNER, S. M. KAST, and J. BRICKMANN*

Institut für Physikalische Chemie, Technische Hochschule Darmstadt, Petersenstrasse 20, D-64287 Darmstadt, Germany

M. SCHLENKRICH

Silicon Graphics, Basel, European Chemistry Technology Center, Kägenstrasse 17, CH-4153 Reinach, Switzerland

Received 1 November 1994; accepted 31 July 1996

ABSTRACT

The calculated Madelung energies and Madelung forces of the electrostatic interaction for nine crystal structures are reported. The method of direct summation with two different shifted-force potentials is compared to the Ewald summation. There is a considerable difference in the convergence of the energy and the force for the two shifted-force potentials regarding the cutoff radius. The convergence depends not only on the potential itself, but also on the crystal structure. One of the shifted-force potentials used is implemented in the CHARMM force field. The energy calculated with this potential shows a good convergence for small cutoff radii. With the other shifted-force potential, the force shows a better convergence for small cutoff radii. The number of pair

* Author to whom all correspondence should be addressed. Prof. Brickmann is also affiliated with Darmstädter Zentrum für Wissenschaftliches Rechnen, Technische Hochschule Darmstadt, Darmstadt, Germany.

Journal of Computational Chemistry, Vol. 18, No. 5, 660–676 (1997)

CCC 0192-8651 / 97 / 050660-17

interactions for obtaining the Madelung limit using the Ewald summation and the direct summation of a shifted-force potential is also reported. For complex structures like zeolites, the number of relevant pair interactions is smaller using the direct summation of a shifted-force potential. For simple structures such as cesium chloride, the number of significant pair interactions is smaller using the Ewald summation.

Introduction

The calculation of long-range electrostatic interactions is the most time-consuming part of molecular dynamics (MD) and Monte Carlo (MC) simulations. In systems with charged particles, the biggest amount of computing time is spent in calculating nonbonded intermolecular forces of the electrostatic interactions. For the exact calculation of electrostatic interactions in solids some methods exist, but the Ewald summation[1] (ES), which was improved by Nijboer and de Wette[2] and Williams,[3] is the only possible one in MD simulations. Other methods like those of Evjen[4] are only practical if the exact crystal structure, for which one has to create a neutral and multipole-free unit cell, is known. This is only possible for simple structures like sodium chloride or cesium chloride. Another alternative is the cell multipole method[5,6] (CMM). This method will become more attractive when the availability of powerful parallel computers increases. A disadvantage of the ES is the effort for the implementation of the code. Furthermore, in MD simulations of bulk systems with no long-range order (e.g., disordered liquids), the ES may produce artificial periodic electrostatic interactions as a consequence of the introduction of periodic boundary conditions in such simulations.

To diminish the number of electrostatic interactions in MD simulations, within the framework of radial direct summation (DS), there are two possibilities that use the cutoff scheme. In this scheme interactions are taken into account within a sphere of cutoff radius r_{cut} and neglected outside. One possibility is simply to truncate the Coulomb interactions at r_{cut} and perform the direct summation of Coulomb terms within the range zero and r_{cut}. Thus, the energy has the finite value $q_i \cdot q_j / r_{\mathrm{cut}}$ at the cutoff radius r_{cut}. Another method is to multiply the usual Coulomb potential by a shifting function $S_{r_{\mathrm{cut}}}(r_{ij})$, which decreases continuously from one to zero within the range zero and r_{cut}:

$$E_{r_{\mathrm{cut}}}(r_{ij}) = \begin{cases} \dfrac{q_i \cdot q_j}{r_{ij}} \cdot S_{r_{\mathrm{cut}}}(r_{ij}), & r_{ij} < r_{\mathrm{cut}} \\ 0, & r_{ij} \geq r_{\mathrm{cut}}. \end{cases} \tag{1}$$

In this case the energy reaches zero at r_{cut}.

Two conditions must be met for such potentials:

$$E_{r_{\mathrm{cut}}}(r)\big|_{r=r_{\mathrm{cut}}} = 0, \tag{2}$$

$$F_{r_{\mathrm{cut}}}(r)\big|_{r=r_{\mathrm{cut}}} = 0, \tag{3}$$

with

$$F_{r_{\mathrm{cut}}}(r) = -\nabla E_{r_{\mathrm{cut}}}(r), \tag{4}$$

where $F_{r_{\mathrm{cut}}}(r)$ is the shifted force. Potentials that do not fulfill these conditions lead to instabilities in the numerical solution of the equations of motion, due to the abrupt impulse induced by a new atom entering the interaction sphere with a nonzero force. As a consequence momentum and energy conservation fail and the system temperature increases steadily.[7,8] Condition (3) is fulfilled if

$$E_{r_{\mathrm{cut}}}(r_{ij}) = \frac{\Omega}{r_{ij}^m} S^E_{r_{\mathrm{cut}}}(r^*) \tag{5}$$

and

$$\begin{aligned} F_{r_{\mathrm{cut}}}(r_{ij}) &= -\nabla E_{r_{\mathrm{cut}}}(r_{ij}) \\ &= \frac{\Omega}{r_{ij}^{m+1}} \left(m \cdot S^E_{r_{\mathrm{cut}}}(r^*) - r_{ij} \cdot \frac{\partial S^E_{r_{\mathrm{cut}}}(r^*)}{\partial r_{ij}} \right), \\ \Leftrightarrow F_{r_{\mathrm{cut}}}(r_{ij}) &= \frac{\Omega}{r_{ij}^{m+1}} S^F_{r_{\mathrm{cut}}}(r^*), \end{aligned} \tag{6}$$

where r^* is a reduced distance r_{ij}/r_{cut}; Ω is a set of parameters, e.g., $q_i \cdot q_j$ for electrostatics; m is 1 for electrostatic interactions, and 6, 12 for the dispersion and the repulsive part of the Lennard–Jones potential; $S^E_{r_{\mathrm{cut}}}(r^*)$ is the shifting function for the energy, and $S^F_{r_{\mathrm{cut}}}(r^*)$ is the shifting function for

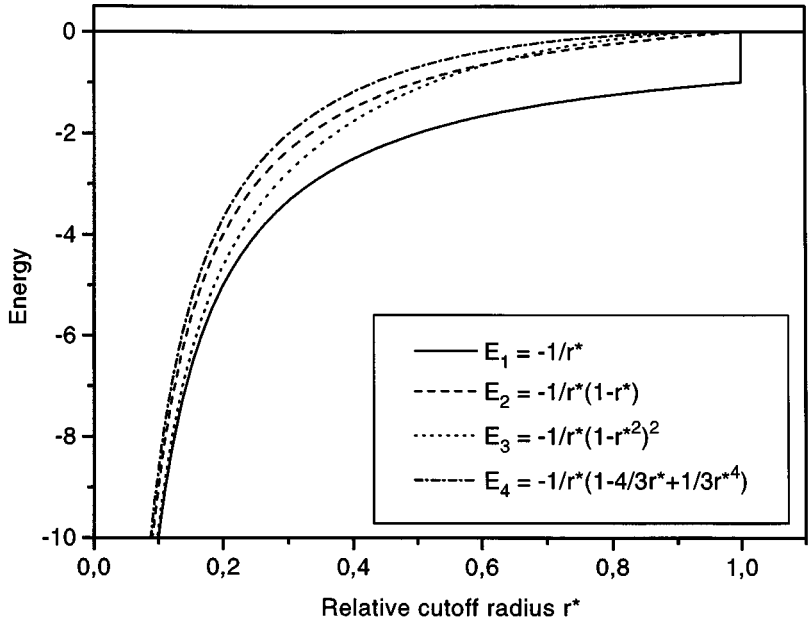

FIGURE 1. Different truncated Coulomb potentials, r^* is the relative distance to an arbitrary cutoff radius r_{cut}: $r^* = r/r_{cut}$, E_1 is a simple Coulomb potential truncated at r_{cut}, E_2 is a shifted potential for which the force at r_{cut} is not zero, E_3 is the CHARMM potential (SFP1),[9] and E_4 is the potential developed by Schrimpf et al. (SFP2).[10]

the force, with

$$S_{r_{cut}}(0) = 1,$$
$$S_{r_{cut}}(r_{cut}) = 0. \tag{7}$$

Figure 1 shows different potentials for calculating the Coulomb energy: a simple truncation of the Coulomb potential r^{-1} at r_{cut} (E_1). In this case conditions (2) and (3) are not met; a shifted potential, for which only condition (3) is met (E_2, the force at r_{cut} is the same as for E_1: $-r_{cut}^{-2}$):

$$E_{r_{cut}}(r_{ij}) = \begin{cases} E(r_{ij}) - E(r_{cut}) \\ \quad = \dfrac{q_i \cdot q_j}{r_{ij}}\left[1 - \dfrac{r_{ij}}{r_{cut}}\right], & r_{ij} < r_{cut} \\ 0, & r_{ij} \geq r_{cut}; \end{cases} \tag{8}$$

the shifted-force potential (SFP) that is implemented, for example, in the CHARMM program[9] (E_3) that reads

$$E_{r_{cut}}(r_{ij}) = \begin{cases} \dfrac{q_i \cdot q_j}{r_{ij}}\left[1 - \left(\dfrac{r_{ij}}{r_{cut}}\right)^2\right]^2, & r_{ij} < r_{cut} \\ 0, & r_{ij} \geq r_{cut}, \end{cases} \tag{9a}$$

$$F_{r_{cut}}(r_{ij}) = \begin{cases} \dfrac{q_i \cdot q_j}{r_{ij}^2}\left[1 + 2\left(\dfrac{r_{ij}}{r_{cut}}\right)^2 - 3\left(\dfrac{r_{ij}}{r_{cut}}\right)^4\right], & r_{ij} < r_{cut} \\ 0, & r_{ij} \geq r_{cut}; \end{cases} \tag{9b}$$

the SFP of Schrimpf et al.[10] (E_4) that has the form

$$E_{r_{cut}}(r_{ij}) = \begin{cases} \dfrac{q_i \cdot q_j}{r_{ij}}\left[1 - \dfrac{4}{3}\dfrac{r_{ij}}{r_{cut}} + \dfrac{1}{3}\left(\dfrac{r_{ij}}{r_{cut}}\right)^4\right], & r_{ij} < r_{cut} \\ 0, & r_{ij} \geq r_{cut}, \end{cases} \tag{10a}$$

$$F_{r_{cut}}(r_{ij}) = \begin{cases} \dfrac{q_i \cdot q_j}{r_{ij}^2}\left[1 - \left(\dfrac{r_{ij}}{r_{cut}}\right)^4\right], & r_{ij} < r_{cut} \\ 0, & r_{ij} \geq r_{cut}. \end{cases} \tag{10b}$$

Potentials and forces (9) and (10) meet conditions (2) and (3).

The radial DS of SFP (DS-SFP) is a standard method in MD simualtions and was used for the first time by Street et al.[11] and Nicolas et al.[12] for

the simulation of Lennard–Jones liquids. Because of the fact that the computing time in an MD simulation is roughly proportional to the number of pair interactions (NPI),

$$\mathrm{NPI} = \frac{N(n-1)}{2} \approx \frac{N \cdot n}{2}, \quad n = \rho_N V(r_{\mathrm{cut}}) < N$$

$$\Rightarrow \frac{d\,\mathrm{NPI}(r_{\mathrm{cut}})}{dr_{\mathrm{cut}}} \approx 2N\pi\rho_N r_{\mathrm{cut}}^2, \qquad (11)$$

where N is the number of particles in the system; n the number of particles in the sphere V with radius r_{cut}, ρ_N the particle density; and due to the r_{cut}^2 dependence of the change of NPI [eq. (11)], a small r_{cut} is preferred. In MD simulations r_{cut} is restricted to a limited range because of the conditions of the simulation (periodic boundary conditions, MD box size).

In many cases[13–20] DS-SFP in MD simulations leads to substantially different results in comparison to the experiment. It is generally believed that the ES compared with DS-SFP leads to significantly better results compared to experimental data. However, it is also reported[20] that there are cases in which ES gives in some respects hardly any improvement, particularly when potentials other than Coulomb are also taken into account. The authors relate this to the fact that the force field parameters are optimized for a certain cutoff radius. The cutoff distance itself, therefore, plays the role of a force field parameter. The shortcomings of this method are thus at least partly compensated. Besides the question of suitable functional forms of truncation schemes remains the controversial discussion as to whether to use atom-based or group-based cutoff methods.[13,19,21] Obviously, advantages and disadvantages of either method depend on the observables under study. A generally valid prescription is yet unclear.

In the present work we investigated the convergence behavior of the Madelung energy and Madelung force calculated by DS of two different atom-based SFPs with increasing cutoff radius. These results are compared with those obtained by ES. In contrast to other investigations we performed the calculations on rigid structures without any dynamics in order to be uninfluenced by conditions and parameters of an MD simulation. Thus, the influence of the cutoff radius on the results of the DS-SFP could be directly assessed and the result was not contaminated by other effects of the simulation. The number of pair interactions necessary to reach the Madelung limit for ES and the DS-SFP were also compared. Energy and force were treated separately. Calculations for nine crystal structures are reported: cesium chloride, β-silver iodide,[22] sodium chloride, rutile,[23] α-corundum,[24] zeolite ZSM-5,[25] zeolite Y (aluminum free),[26] and zeolite Na-Y with Si/Al ratio 1:1 and 3:1 [subsequently indicated as Na-Y (1:1) and Na-Y (3:1)].[26]

Methods

We used the ES procedure based on the algorithm of Karasawa and Goddard.[27] The SFPs under study were the CHARMM shift function,[9] eq. (9) (subsequently termed SFP1), and the one developed in our group,[10] eq. (10) (subsequently termed SFP2). To measure the difference between the ES and the DS of SFP1 and SFP2, several descriptors were computed: the mean relative deviation Δ_x for the Madelung energy and for the absolute value of the Madelung force

$$\Delta_x = \frac{1}{N}\sum_i^N \frac{x_i^{\mathrm{DS\text{-}SFP}} - x_i^{\mathrm{ES}}}{x_i^{\mathrm{ES}}}, \qquad (12)$$

where x is the Madelung energy or the absolute value of the Madelung force and i is the atom index; the angle θ between the Madelung forces is calculated by DS and by ES,

$$\theta = \frac{1}{N}\sum_i^N \frac{\theta_i^{\mathrm{DS\text{-}SFP}} - \theta_i^{\mathrm{ES}}}{\theta_i^{\mathrm{ES}}}, \qquad (13)$$

with

$$\cos\theta_i = \frac{|\mathbf{F}_i^{\mathrm{ES}} \cdot \mathbf{F}_i^{\mathrm{DS\text{-}SFP}}|}{|\mathbf{F}_i^{\mathrm{ES}}| \cdot |\mathbf{F}_i^{\mathrm{DS\text{-}SFP}}|}. \qquad (14)$$

The angle zero indicates that there is no difference in the direction of the forces calculated with both methods, and the angle 180° means the two forces have opposite directions. The calculations were performed for different cutoff radii r_{cut} in the range of 5–15 Å in steps of 1 Å, 15–30 Å in steps of 5 Å, 30–200 Å in steps of 10 Å, and up to 500 Å in steps of 50 Å. In most MD simulations the cutoff radii in the range between 8 and 12 Å are used.

The ratio of the number of pair interactions (RPI) between the DS and the ES as a function of

the cutoff radius r_{cut} was estimated as

$$\mathrm{RPI}(r_{cut}) = \frac{\mathrm{NPI}^{\mathrm{DS\text{-}SFP}}(r_{cut})}{\mathrm{NPI}^{\mathrm{ES}}}, \qquad (15)$$

where $\mathrm{NPI}^{\mathrm{ES}}$ is the NPI of the ES, and $\mathrm{NPI}^{\mathrm{DS\text{-}SFP}}$ that of the DS-SFP. $\mathrm{NPI}^{\mathrm{DS\text{-}SFP}}$ depends only on r_{cut} and ρ_N and is independent of the functional form of the potential and the crystal structure [see eq. (11)], while $\mathrm{NPI}^{\mathrm{ES}}$ depends only on the crystal structure. Thus, RPI is useful to estimate whether to prefer ES or DS-SFP with respect to minimal computing time. An RPI of 1 corresponds to a structure-specific limit of the cutoff radius for which $\mathrm{NPI}^{\mathrm{DS\text{-}SFP}} = \mathrm{NPI}^{\mathrm{ES}}$. For larger cutoff radii the ES is recommended; for smaller ones the DS is the better choice, independent of the potential. For the energy and the force $\mathrm{NPI}^{\mathrm{DS\text{-}SFP}}$ is equal. Because $\mathrm{NPI}^{\mathrm{ES}}$ is smaller for the force than for the energy (for details see Karasawa and Goddard[27]), $\mathrm{RPI}_{\mathrm{force}}$ is steeper than $\mathrm{RPI}_{\mathrm{energy}}$ with increasing cutoff radius. How much computing time is actually needed depends on the implementation of the algorithms for ES and DS-SFP. Consequently, one has to correct the RPI by the factor $t_{\mathrm{DS\text{-}SFP}}/t_{\mathrm{ES}}$, where t is the computing time for one pair interaction with the corresponding method.

The nine crystal structures of different complexity studied in this work are described in Table I. We used formal charges according to the oxidation number of the respective atoms. This had no effect on $\mathrm{NPI}^{\mathrm{DS\text{-}SFP}}$, because it depends only on r_{cut}. But according to

$$\mathrm{NPI}^{\mathrm{ES}} \propto N \cdot \sum_{i=1}^{N} q_i^2 \qquad (16)$$

of Karasawa and Goddard's algorithm of the ES,[27] the reported RPI are too small and should be regarded as a lower limit, i.e., for smaller charges the RPI increases, favoring ES.

TABLE I.
Crystal Structures Used in This Work.

Crystal Structure	Density of Particles (10^{-2} Å^{-3})	Formal Charges
CsCl	2.86	$Cs^{+I}Cl^{-I}$
β-AgI	2.92	$Ag^{+I}I^{-I}$
Zeolite Y (aluminum free)	3.75	$Si^{+IV}O_2^{-II}$
Zeolite Na-Y (3:1)[a]	4.07	$Na^{+I}[Al^{+III}Si_3^{+IV}O_8^{-II}]$
Zeolite Na-Y (1:1)[a]	4.38	$Na^{+I}[Al^{+III}Si^{+IV}O_4^{-II}]$
NaCl	4.46	$Na^{+I}Cl^{-I}$
Zeolite ZSM-5 (aluminum free)	5.40	$Si^{+IV}O_2^{-II}$
TiO_2	9.61	$Ti^{+IV}O_2^{-II}$
α-Al_2O_3	11.80	$Al_2^{+III}O_3^{-II}$

[a] The rule of Loewenstein[28] is fulfilled. In the ratio Si/Al = 1:1, every Si is coordinated by 4 Al, and vice versa. For the ratio Si/Al = 3:1, the Al are binomially distributed with Loewenstein's rule as the constraint.

Results and Discussion

It is well known that simple DS without an appropriate shifting function does not lead to the correct Madelung (Mad) interaction energy or force as calculated by ES, not even for an infinite cutoff radius, i.e.,

$$\lim_{r_{cut}\to\infty} \sum_{i=1}^{N} \sum_{j>i}^{N} E_{r_{cut}}(r_{ij}) \neq E_{\mathrm{Mad}}. \qquad (17)$$

On the other hand, the DS-SFP converges to the exact Madelung value (calculated by ES),

$$\lim_{r_{cut}\to\infty} \sum_{i=1}^{N} \sum_{j>i}^{N} \frac{q_i \cdot q_j}{r_{ij}} S^E_{r_{cut}}(r_{ij}) = E_{\mathrm{Mad}}. \qquad (18)$$

While there is no general analytic proof for eq. (18), in principle the ES, eq. (19), is similar to the DS-SFP,

$$E_i^{\mathrm{ES}} = q_i \left(\frac{1}{\eta} \sum_{R_L,\, j}^{N} q_j \frac{\mathrm{erfc}\left(|\mathbf{r}_i - \mathbf{r}_j - \mathbf{R}_L|/\eta\right)}{|\mathbf{r}_i - \mathbf{r}_j - \mathbf{R}_L|/\eta} + \frac{4\pi}{\Omega} \sum_{H_L,\, j}^{N} q_j \frac{\cos(\mathbf{H}_L \cdot [\mathbf{r}_i - \mathbf{r}_j])}{\mathbf{H}_L^2 \exp\left(\left[\tfrac{1}{2}\eta|\mathbf{H}_L|\right]^2\right)} \right) - \frac{q_i^2}{\pi^{1/2}\eta}, \qquad (19)$$

where E_i^{ES} is the Madelung energy for particle i, $\mathbf{R}_L$ the translation vector for the real space, $\mathbf{H}_L$ the translation vector for the reciprocal space, η the Ewald parameter, and Ω the unit-cell volume. If the Ewald parameter η in (19) is infinite the whole summation is performed in real space. In this case the error function complement erfc is comparable to a shifting function as in (1), and η corresponds to r_{cut}. So there is good reason for the assumption that eq. (18) is correct, which is supported by numerical analysis in the following.

EXPLICIT NUMERICAL PROOF FOR 1- AND 3-DIMENSIONAL MADELUNG MODELS

1-Dimensional Madelung Model

This known model[29] consists of a chain of point charges with alternating signs and a spacing of one arbitrary unit length. The energy for the positive point charge 1 is then

$$E_1^{\mathrm{ES}} = \lim_{N\to\infty} \sum_{n=1}^{N} \frac{(-1)^n}{n} = -\ln 2, \qquad (20)$$

and the absolute value of the force is

$$F_1^{\mathrm{ES}} = \lim_{N\to\infty} \sum_{n=1}^{N} \frac{(-1)^n}{n^2} = -\frac{\pi}{12}. \qquad (21)$$

Both infinite series are well known.[30] To give a numerical confirmation for eq. (18) the above model was treated with the SFPs, SFP1 and SFP2, yielding

$$E_1^{\text{DS-SFP}} = \lim_{N\to\infty} \sum_{n=1}^{N} \frac{(-1)^n}{n} S_N^E(n) = -\ln 2, \quad (22a)$$

$$F_1^{\text{DS-SFP}} = \lim_{N\to\infty} \sum_{n=1}^{N} \frac{(-1)^n}{n^2} S_N^F(n) = -\frac{\pi}{12}, \quad (22b)$$

with

$$S_N^E(n) = \begin{cases} \left[1 - \left(\frac{n}{N}\right)^2\right]^2 & \text{(SFP1)} \\ \left[1 - \frac{4}{3}\frac{n}{N} + \frac{1}{3}\left(\frac{n}{N}\right)^4\right] & \text{(SFP2)} \end{cases} \qquad (23)$$

and

$$S_N^F(n) = \begin{cases} \left[1 + 2\left(\frac{n}{N}\right)^2 - 3\left(\frac{n}{N}\right)^4\right] & \text{(SFP1)} \\ \left[1 - \left(\frac{n}{N}\right)^4\right] & \text{(SFP2).} \end{cases} \qquad (24)$$

3-Dimensional Madelung Model

In this case the model consists of a 3-dimensional lattice of equidistant point charges with alternating signs. This example of a multipole-free system corresponds to a lattice of the NaCl type with a cation–anion distance of one unit length and a side of the cube of $2N$, where N is the number of shells surrounding the positive point charge at the origin. The summation is performed from zero to infinity; therefore, only one octahedron of the NaCl-like cube is calculated. The expansion from $-\infty$ to $+\infty$ can be done analogously but is more costly than starting at zero. The summation for the energy and force are then defined as (the index 1 refers to the point charge at the origin)

$$E_1 = \lim_{N\to\infty} \sum_{i=0}^{N} \sum_{j=0}^{N} \sum_{k=0}^{N} \frac{(-1)^{i+j+k}}{n} \qquad (25)$$

and

$$F_1 = \lim_{N\to\infty} \sum_{i=0}^{N} \sum_{j=0}^{N} \sum_{k=0}^{N} \frac{(-1)^{i+j+k}}{n^2} \qquad (26)$$

with

$$n^2 = (i^2 + j^2 + k^2) \neq 0. \qquad (27)$$

The results are $E_1 = -1.3445$ and $F_1 = -1.74836$. The same results are obtained for SFP1 and SFP2.

The convergence behavior of eq. (25) for $-N$ to $+N$ calculated with different algorithms is depicted in Figure 2. The limit of the lattice sum, which is shown in the plots as a horizontal line, is -1.747565 according to

$$E = M_\alpha \frac{q_1 \cdot q_2}{\alpha}, \qquad (28)$$

where α is a characteristic length in the crystal, for example, the shortest cation–anion distance, and M_α Madelung's constant. The parameters were set to $q_1 = 1$, $q_2 = -1$, and $\alpha = 1$.

The algorithm used for Figure 2a–c contains a summation within an *outscribed* sphere with a cutoff radius that corresponds to half the diagonal of the NaCl-like cube (formally $3^{1/2}N$), and therefore includes all particles of the cube. Figure 2a shows the sum of the multipole-free model with the total charge corresponding to $(-1)^N$. The model corresponding to Figure 2b is also multipole-free and neutral. Neutrality is accomplished by assigning only a fraction of a charge to particles located at

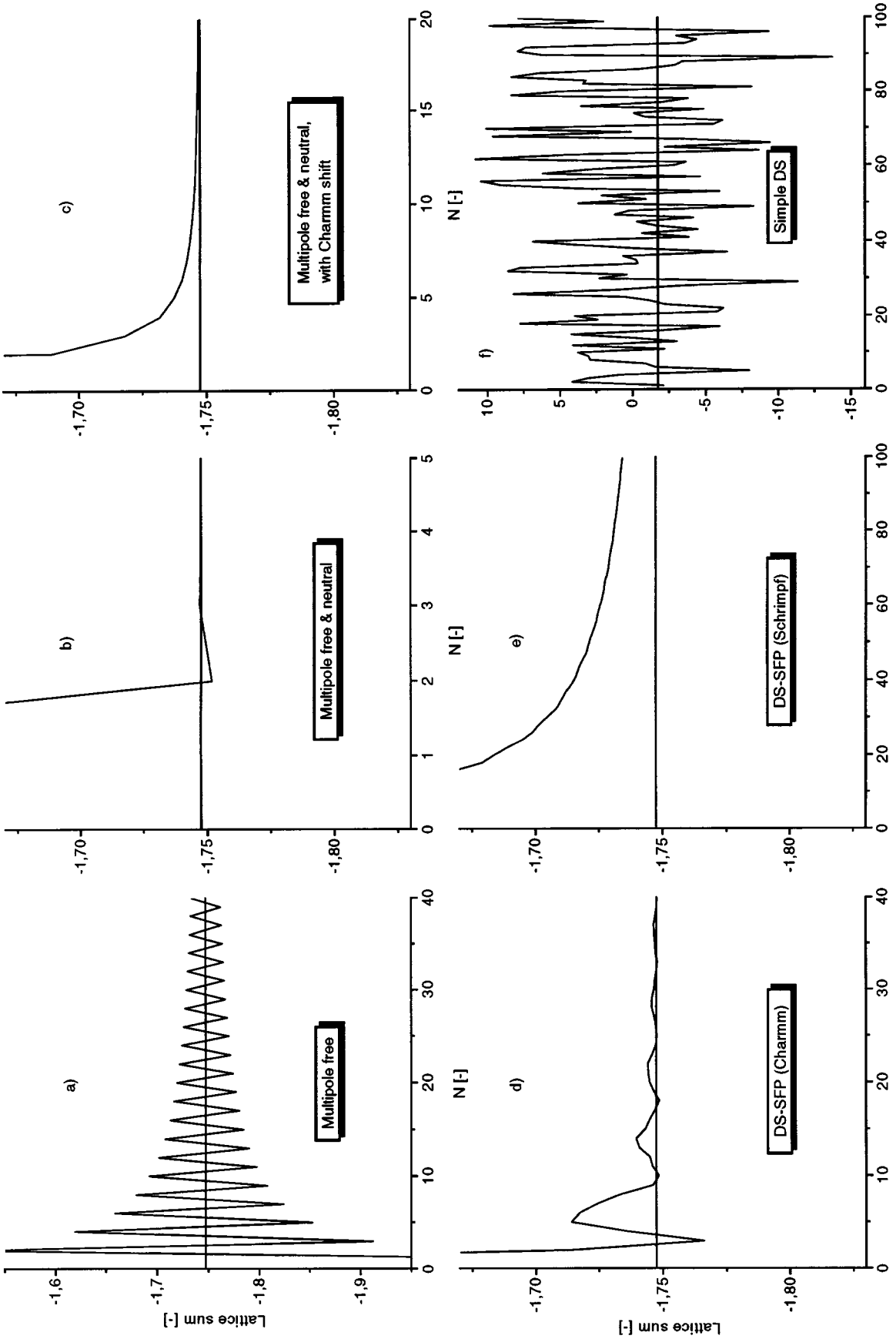

FIGURE 2. Different summation algorithms for calculating the lattice sum of an NaCl-type lattice: (a) charged multipole-free model, (b) neutral multipole-free model according to Evjen,[4] (c) Evjen model with the shifting function $S_N^E(n)$ of SFP1, (d, e) direct summation of shifted-force potentials with both investigated shifted-force potentials, and (f) direct summation of an unshifted Coulomb potential.

the outermost sphere. The charge of a particle on a face, edge, and corner is weighted by 1/2, 1/4, and 1/8, respectively. For this model Evjen[4] proved that the summation definitely converges. The summation for Figure 2c is the same as for 2b except that the single Coulomb terms are multiplied by the shifting function $S_N^E(n)$ of SFP1 [see eq. (22) for the 1-dimensional model].

The algorithm used for Figure 2d–f contains a summation within an *inscribed* sphere with a cut-off radius that corresponds to half of the side of the NaCl-like cube (formally N), and therefore includes only a fraction of the particles of the cube. This is the principle of a radial DS as used in MD simulations. Figure 2d, e shows the DS-SFP with SFP1 and SFP2, respectively. The simple DS of the

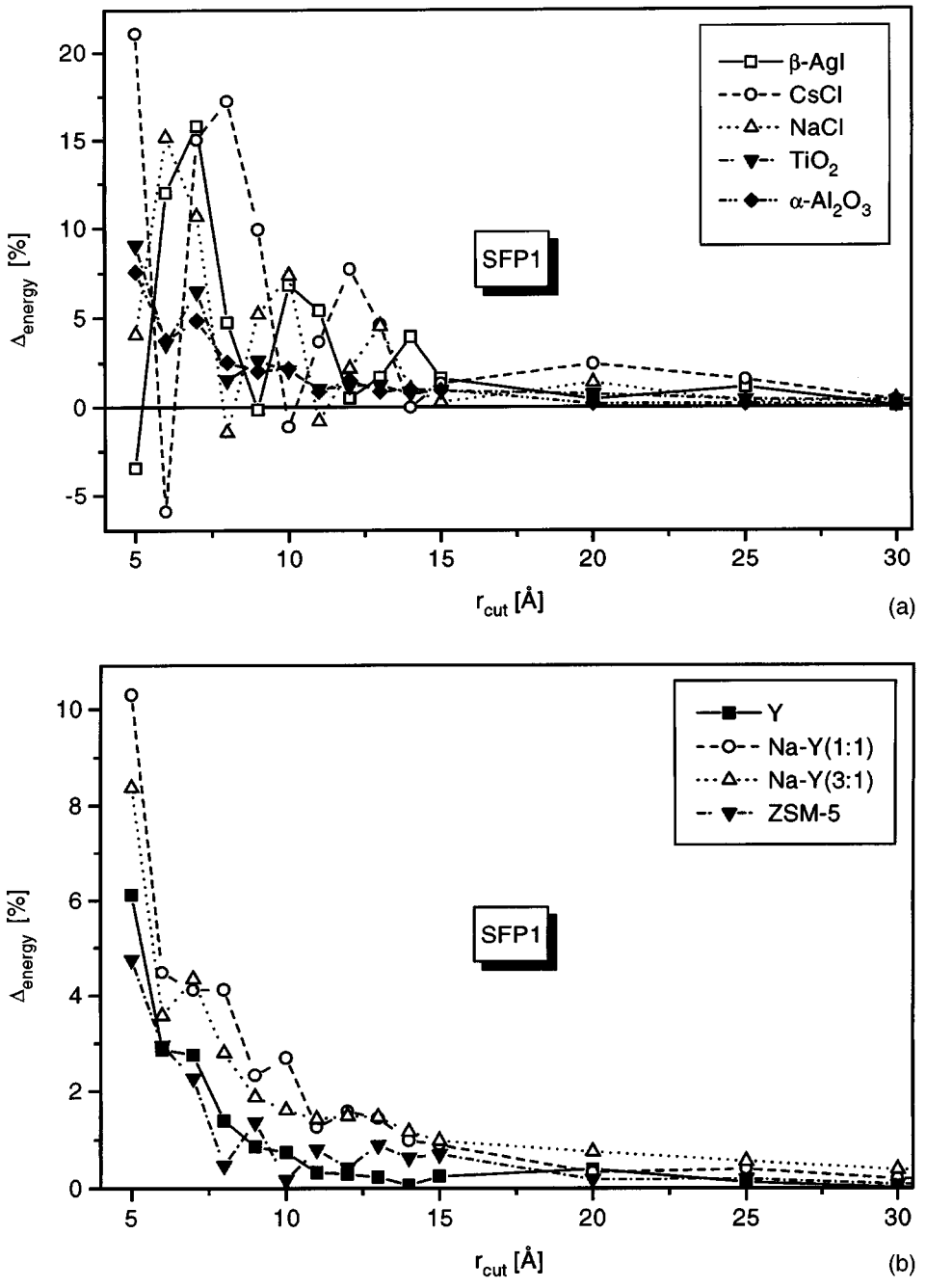

FIGURE 3. The relative deviation Δ_{energy} between ES and DS-SFP calculated for the energy with SFP1 for (a) nonzeolites and (b) zeolites.

Coulomb potential without any shifting function is depicted in Figure 2f.

These examples demonstrate the convergence of Madelung interactions using SFPs. For neutral and multipole-free systems (''Evjen models''), the convergence is extremely good (Fig. 2b). The Madelung limit is already reached for $N = 4$. As mentioned above, such models are not realistic for MD simulations. As depicted in Figure 2d, e, for radial DS-SFP the convergence depends significantly on the shifting function. A simple unshifted Coulomb potential does not yield any convergence (Fig. 2f).

NUMERICAL CALCULATIONS FOR NINE CRYSTAL STRUCTURES

The results of the following numerical calculations clearly show the dependence of the convergence of the Madelung interactions on the crystal structures and on the type of the SFP.

Δ_{energy} for Madelung Energy

As shown in Figure 3 for SFP1 and in Figure 4 for SFP2, Δ_{energy} [eq. (12)] for SFP2 is considerably smoother and more monotonic but not as steep as for SFP1. Δ_{energy} calculated with SFP1 fluctuates intensely below a cutoff radius of 12 Å. For SFP2, Δ_{energy} clearly converges slower with increasing cutoff radius. For the zeolites, Δ_{energy} falls below 2% in the 7–10 Å range; the same is true for TiO_2 and α-Al_2O_3 at a cutoff radius of 10 Å using SFP1. Δ_{energy}, calculated with SFP2, falls below 10% in the 13–15 Å range for the zeolites; the same is true for TiO_2 and α-Al_2O_3 at a cutoff radius of 15 Å. For the other simple compounds like CsCl, NaCl, and β-AgI, Δ_{energy} behaves similarly but is shifted approximately 5 Å to larger cutoff radii compared to TiO_2 and α-Al_2O_3. For small cutoff radii, the fluctuation of Δ_{energy} of the simple structures is more pronounced than for zeolites, TiO_2, or α-Al_2O_3. For simple structures and SFP1 it is not possible to determine a definite cutoff limit less than 12 Å for which Δ_{energy} is continuously below a certain small value because of the fluctuations (Fig. 3a). An appropriate cutoff radius has to be determined from case to case. The convergence of the Madelung energy also depends on the crystal structure. Concerning a maximum deviation of 2% the following cutoff radii are necessary for SFP1: ZSM-5, Y, and Na-Y (3:1), 7–8 Å; TiO_2, α-Al_2O_3, and Na-Y (1:1), 10 Å; NaCl and β-AgI, 13–14 Å; and CsCl, 20 Å. For example, at 12 Å Δ_{energy} is 7.7% for CsCl and 0.3% for the Y zeolite. Again, for simple structures Δ_{energy} shows worse convergence behavior, whereas for complex structures such as zeolites it shows faster and smoother convergence with increasing cutoff radius. Above a cutoff radius of 20 Å the deviations are smaller than 2% for all compounds. The deviations decrease to less than 0.05% for cutoff radii above 100 Å. This is not true for α-Al_2O_3, for which the smallest deviation is 0.12% at 30 Å and then it increases slowly to an approximate limit of 0.44% at 500 Å. Measured by Δ_{energy} this compound shows the slowest convergence of all structures and does not seem to converge to the same Madelung limit calculated with ES.

Δ_{force} for Madelung Force

Forces that have to be zero due to the crystal symmetry are in fact calculated as zero even for small cutoff radii independent of the potential used. The forces for all atoms in CsCl, NaCl, all titanium atoms in TiO_2, and the x and y components of all atoms in β-AgI are zero. For the latter the z components of silver and iodine necessarily have opposite signs.

In general, Δ_{force} [eq. (12)] is larger than Δ_{energy} and it fluctuates for both SFPs used (Fig. 5 for SFP1 and Fig. 6 for SFP2). Regarding the absolute value of the forces, the shapes of the curves are almost equal for both SFPs used with one and the same crystal structure. For SFP2, Δ_{force} is smaller and converges faster than for SFP1. For example, Δ_{force} of Y zeolite falls below 4% at a cutoff distance of 6 Å using SFP2 whereas with SFP1 this happens at 15 Å. There is bad force convergence for simple structures. The following values are reported for SFP2 (the values for SFP1 are clearly larger): for β-AgI Δ_{force} is 120.5% at 10 Å and still 5.4% at 90 Å. For α-Al_2O_3 Δ_{force} behaves analogously to the energy. First it converges to smaller values (−0.38% at 30 Å) and then increases to 18–20% within a range of 450 and 500 Å. With SFP1 the latter value is 3.8 times higher. For Na-Y (1:1) Δ_{force} fluctuates strongly and converges more slowly compared to other zeolites.

The angle θ [eq. (13)] exhibits the same behavior as the absolute value of the force with regard to the choice of SFPs and the complexity of crystal structures (Fig. 7 for SFP1 and Fig. 8 for SFP2). Within 11–15 Å, θ goes up to 2.9° for the zeolites with SFP2 and up to 7° with SFP1. For β-AgI, θ changes between the two angles (0° and 180°) below 15 Å. For TiO_2, θ has a maximum of 2°. For

α-Al_2O_3, the angle θ shows analogous behavior like the absolute value of the force. θ has a minimum of 4.7° at 14 Å and reaches about 30° at 500 Å (60° for SFP1).

In principle, we found the following rule of thumb: the smaller the deviations of the forces, the larger the deviations of the energies, and vice versa.

RPI

As depicted in Figure 9 there is no proportionality between ρ_N and the RPI, although the $NPI^{DS\text{-}SFP}$ increases linearly with ρ_N. For example, α-Al_2O_3 has the highest density of all investigated structures, but for all other structures the RPI is much higher (except the zeolites). Additionally CsCl with the lowest density has the highest RPI. This is due

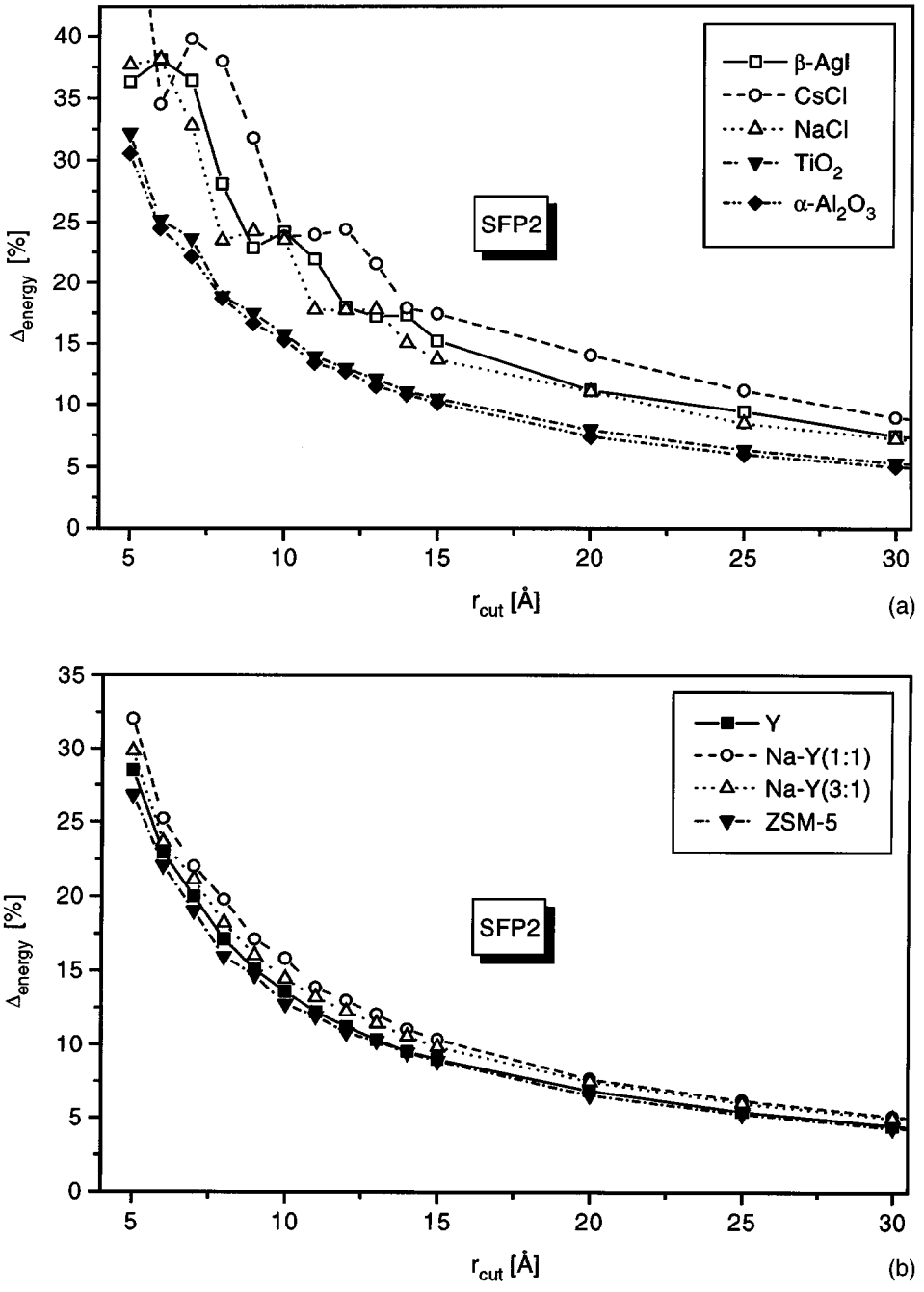

FIGURE 4. The relative deviation Δ_{energy} between ES and DS-SFP calculated for the energy with SFP2 for (a) nonzeolites and (b) zeolites.

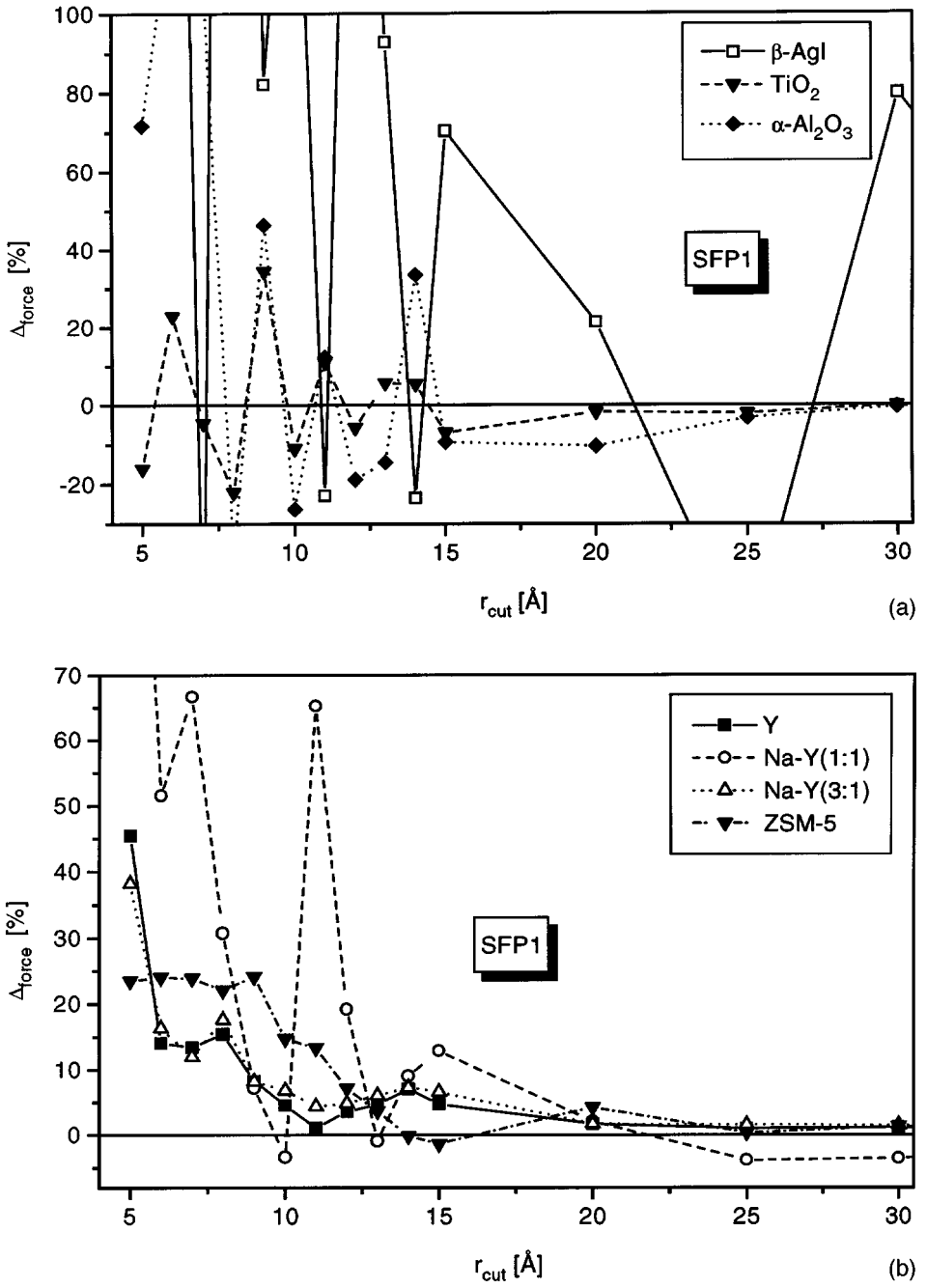

FIGURE 5. The relative deviation Δ_{force} between ES and DS-SFP calculated for the absolute value of the force with SFP1 for (a) nonzeolites and (b) zeolites.

to the structural dependence of the ES. While the NPI^{ES} for CsCl is only 128, for α-Al_2O_3 it is 92098; therefore, the RPI for α-Al_2O_3 is smaller than the RPI for CsCl. Again the complexity of the structure is the predominant factor; as a rough approximation, the more complex structure, the smaller the RPI for a specific cutoff radius. Zeolites show the smallest RPI of all considered substances. For a cutoff radius of 12 Å, the RPI_{energy} is $3.5 \cdot 10^{-3}$ and the RPI_{force} is $4.5 \cdot 10^{-3}$ for the Faujasite-type zeolites, which means the DS-SFP is about 222–286 times faster than the ES concerning the NPI. Even for a cutoff radius of 25 Å (which is approximately the cell parameter of the Faujasite-type zeolites), the RPI_{energy} is 0.033 and RPI_{force} is 0.043; for a cutoff radius of 50 Å, the $RPI_{energy,\ force}$ is still

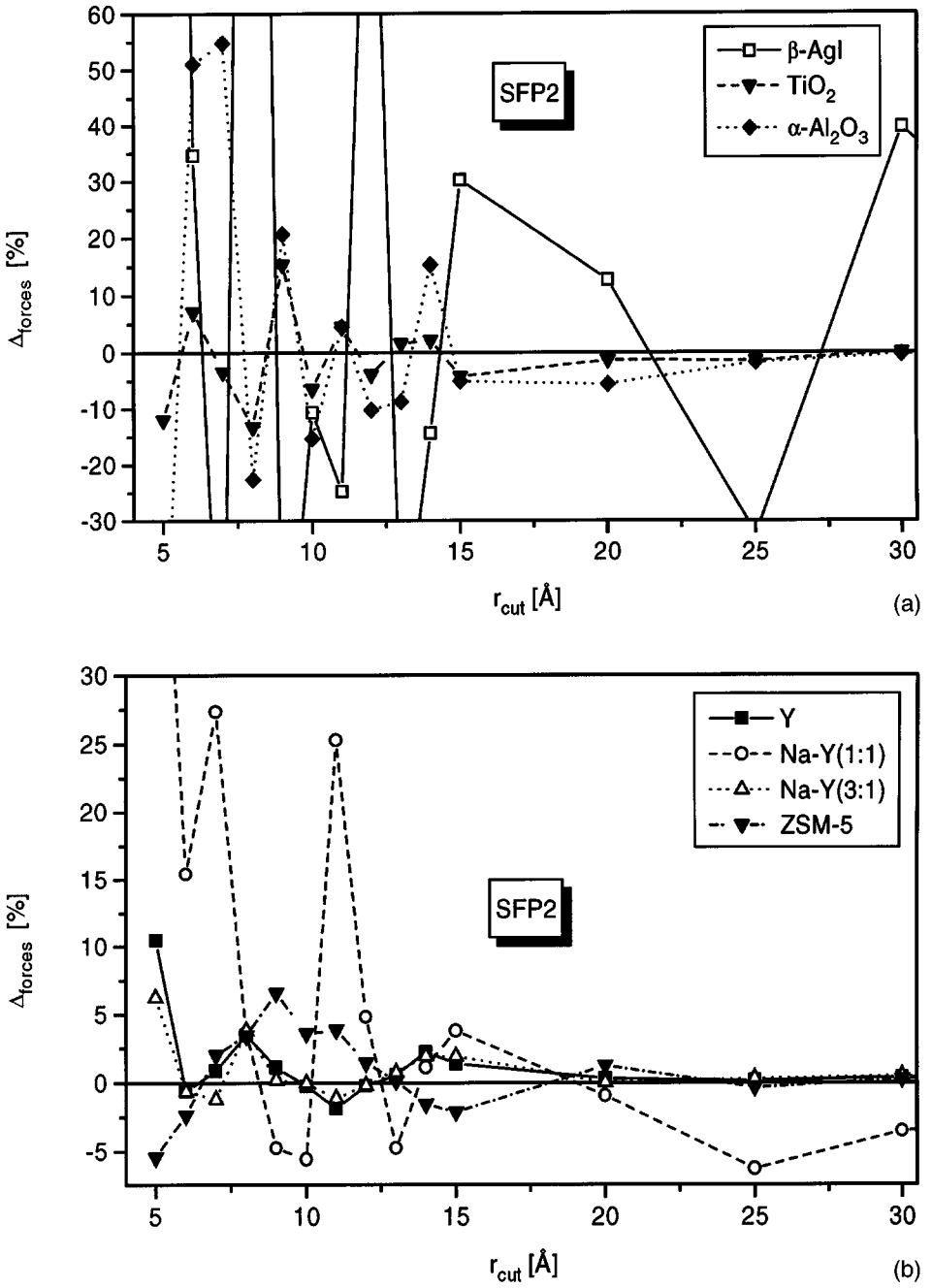

FIGURE 6. The relative deviation Δ_{force} between ES and DS-SFP calculated for the absolute value of the force with SFP2 for (a) nonzeolites and (b) zeolites.

below 1.0. Also the RPI of α-Al_2O_3 is smaller than the RPI of the other nonzeolites ($RPI_{energy} = 0.6$, $RPI_{force} = 0.8$ for $r_{cut} = 20$ Å). The RPI is not the only factor used in deciding whether to use DS-SFP or ES. If the computing time is important and considering the small values of Δ_{energy} and Δ_{force} for the zeolites and α-Al_2O_3, only the direct DS-SFP is reasonable for these structures. For TiO_2 and β-AgI it depends on whether it is necessary to calculate the energy or the force (TiO_2: $RPI_{energy} > 0.6$ and $RPI_{force} > 1.9$ for $\Delta_{energy,\ force} < 2\%$). For β-AgI a minimum cutoff radius of 14 Å for the energy and more than 90 Å for the force is required ($\Delta_{energy,\ force} < 2\%$). This corresponds to $RPI_{energy} = 0.8$ and $RPI_{force} = 329$. For CsCl, at least a cutoff radius of 20 Å is necessary for $\Delta_{energy} <$

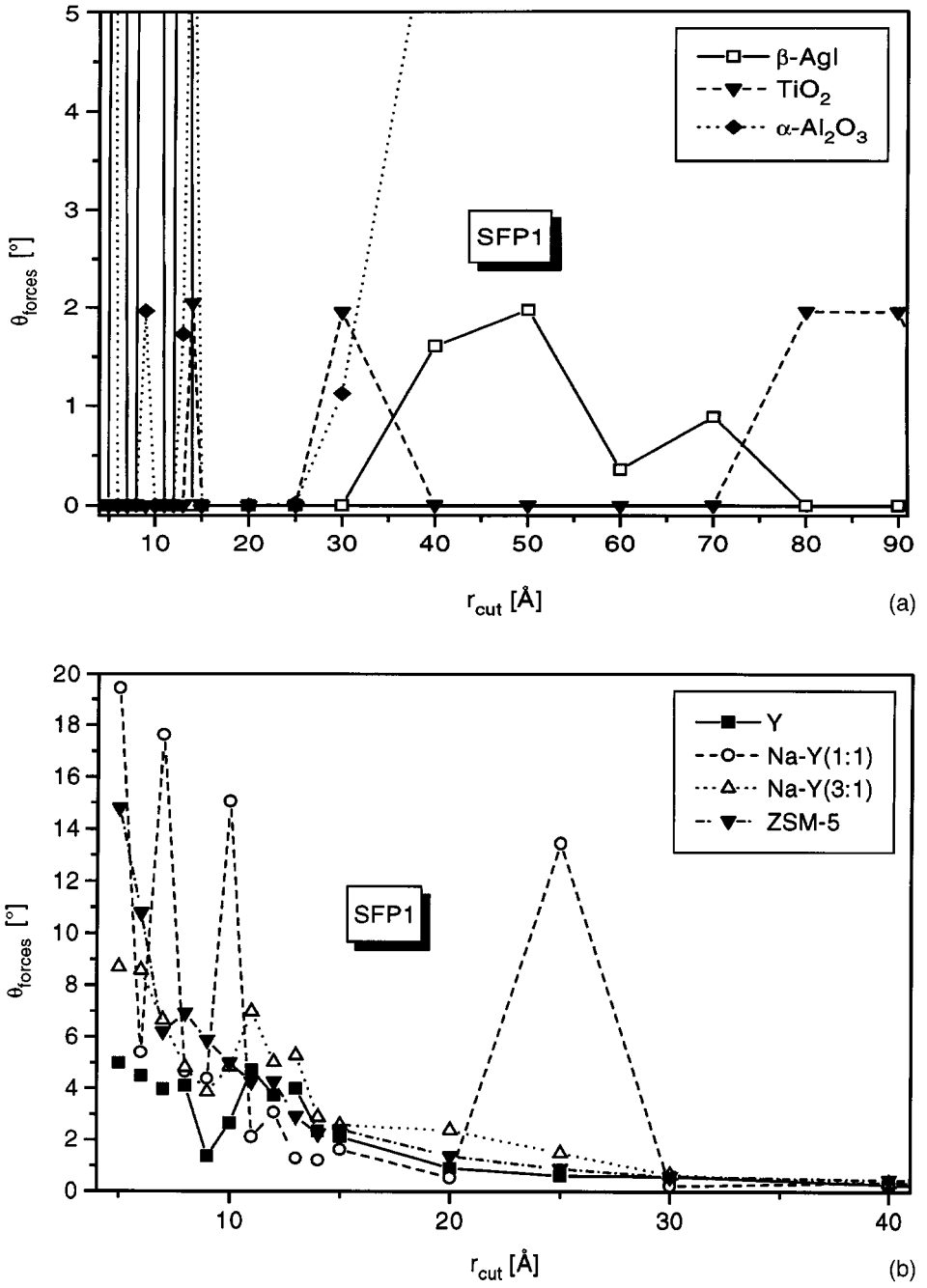

FIGURE 7. Angle θ between the forces of ES and DS-SFP with SFP1 for (a) nonzeolites and (b) zeolites.

2%, which means the RPI is larger than 7.3. Consequently for simple structures only the use of ES is reasonable. The results are combined in Table II. A selected value of 2% for $\Delta_{\text{energy, force}}$ significantly demonstrates the difference between the zeolites and the nonzeolitic structures.

Conclusions

Because of computing-time restrictions and for other practical reasons, MD simulations of solids are mainly performed with finite cutoff radii to keep the NPI small. In this situation SFPs are

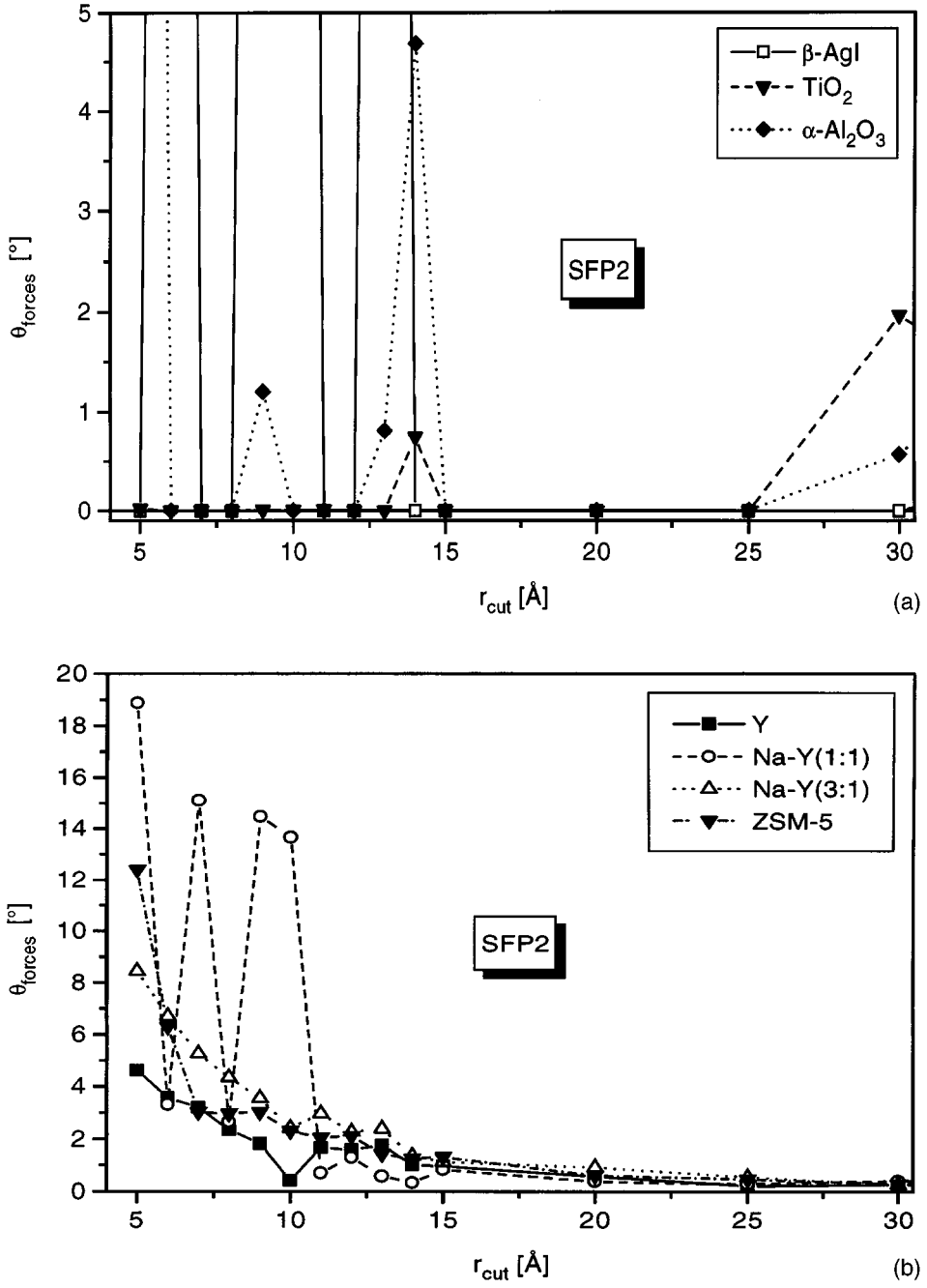

FIGURE 8. Angle θ between the forces of ES and DS-SFP with SFP2 for (a) nonzeolites and (b) zeolites.

essential for energy and momentum conservation. Compared to the ES the DS-SFP causes an error that is a function of the cutoff radii and crystal structure.

We have shown that the DS-SFP and the ES lead to nearly identical results for large cutoff radii, r_{cut}. Nevertheless, it is not possible to explain the poor convergence of α-Al_2O_3 for large cutoff radii.

The regarded SFPs differ considerably with respect to the calculation of Madelung interactions. The energies calculated with the SFP1 converge faster with respect to the cutoff radii than the energies calculated with SFP2. On the other hand, energies calculated with SFP2 show monotonic and smoother convergence behavior whereas with SFP1 they oscillate strongly for small cutoff radii. For

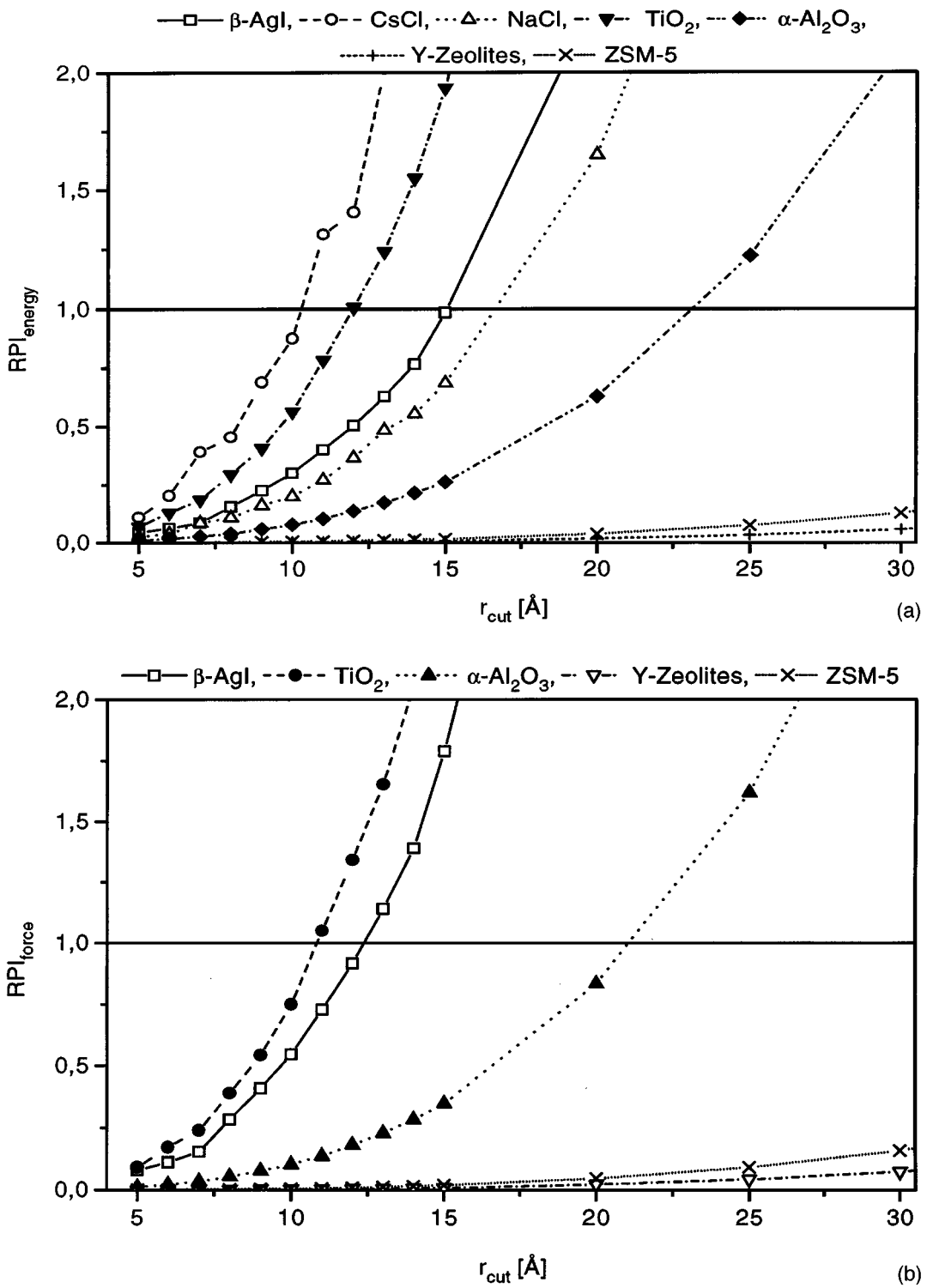

FIGURE 9. Ratio of pair interactions of DS-SFP and ES for (a) the energy and (b) the force.

TABLE II.
Cutoff Radii and Corresponding RPI for Nine Crystal Structures.

Crystal Structures	Energy		Force	
	r_{cut} (Å)	RPI	r_{cut} (Å)	RPI
CsCl	20	7.3	—	—
β-AgI	14	0.8	90	328.7
NaCl	13	0.5	—	—
TiO_2	10	0.6	15	1.9
α-Al_2O_3	10	0.08	20[a]	0.8
Zeolite Y (aluminum free)	7	$8.0 \cdot 10^{-4}$	9[b]	$2.1 \cdot 10^{-3}$
Zeolite Na-Y (3:1)	8	$1.2 \cdot 10^{-3}$	8	$1.5 \cdot 10^{-3}$
Zeolite Na-Y (1:1)	10	$2.0 \cdot 10^{-3}$	13[c]	$5.9 \cdot 10^{-3}$
Zeolite ZSM-5 (aluminum free)	7	$1.6 \cdot 10^{-3}$	11[d]	$7.7 \cdot 10^{-3}$

To show the significant difference between the zeolites and the other crystal structures a small $\Delta_{energy,\,force}$ was chosen ($< 2\%$), which belongs to the reported cutoff radii.
[a] $\Delta_{force} > 2\%$ above 50 Å.
[b] $\Delta_{force} = 2.2$ at 14. Å.
[c] $\Delta_{force} < 4\%$.
[d] $\Delta_{force} = 2.1$ at 15 Å.

the energy a significant dependence on the crystal structure is also found. In particular, complex structures such as zeolites show fast and very smooth convergence of the energy with increasing cutoff distance; for simple structures like CsCl or β-AgI the energy fluctuates strongly and converges more slowly with respect to the cutoff radius. In principle, the deviations of the forces between the DS-SFP and the ES are significantly larger than those for the energies and the convergence behavior is no longer monotonic for both potentials, even for zeolites. Nevertheless, for SFP2 the forces show better convergence with increasing cutoff radius. A decision on using SFP1 or SFP2 has to be made from case to case.

Regarding the RPI there is in general no need to use ES for zeolites. For complex structures a DS-SFP is preferable to an ES due to much shorter computing times and only small deviations. For simple structures ES is better than DS-SFP. SFP2 and a cutoff radius for 10 Å was successfully used by Schrimpf et al. for the MD simulations of Na-Y (3:1).[10]

Of course these results are strictly valid for solid-state calculations only and are not directly transferable to liquids and other disordered systems. In this situation ES introduces artificial periodicity and DS is preferable as long as the used shifting function and cutoff distance cause negligible errors.

The question whether to use approximations that better represent either the potential energy or the forces remains controversial. Obviously, for the integration of the equations of motion only the forces are essential. But the calculation of energy-dependent observables from molecular simulations is equally important. Consistent results from MD simulations can be obtained if the error in force *and* energy calculations is roughly the same. For MC simulations energy accuracy is the key determinant. *A priori* for a given cutoff, it is unclear whether the criterion of equal force and energy accuracy is fulfilled. Further studies are needed to reveal the influence on resulting observables.

Acknowledgments

The numerical proofs were assisted by the *Mathematica* program.[31] This work was supported by the Fonds der Chemischen Industrie, Frankfurt, and partly supported by AKZO Research Laboratories, Obernburg. This work was part of the doctoral thesis of Hagen Dufner, Technische Hochschule Darmstadt (D17).

References

1. P. P. Ewald, *Ann. Phys.*, **64**, 253 (1921).
2. B. R. A. Nijboer and F. W. de Wette, *Physica*, **23**, 309 (1957).
3. D. E. Williams, *Acta Crystallogr., Sect. A*, **27**, 452 (1971).
4. H. M. Evjen, *Phys. Rev.*, **39**, 675 (1932).
5. J. A. Board, Jr., J. W. Cansey, J. F. Leathium, Jr., A. Windemuth, and K. Schulten, *Chem. Phys. Lett.*, **198**, 89 (1992).
6. H.-Q. Ding, N. Karasawa, and W. A. Goddard III, *J. Chem. Phys.*, **97**, 4309 (1992).
7. T. A. Andrea, W. C. Swope, and H. C. Andersen, *J. Chem. Phys.*, **79**, 4576 (1983).
8. D. B. Kitchen, F. Hirata, J. D. Westbrook, R. Levy, D. Kofke, and M. Yarmush, *J. Comp. Chem.*, **11**, 1169 (1990).
9. (a) B. R. Brooks, R. E. Bruccoleri, B. D. Olafson, D. J. States, S. Swaminathan, and M. Karplus, *J. Comp. Chem.*, **4**, 187 (1983); (b) L. Nilsson and M. Karplus, *J. Comp. Chem.*, **7**, 591 (1986).
10. G. Schrimpf, M. Schlenkrich, J. Brickmann, and P. A. Bopp, *J. Phys. Chem.*, **96**, 7404 (1992).

11. W. B. Streett, D. J. Tildesley, and G. Saville, *ACS Symp. Ser.*, **86**, 144 (1978).
12. J. J. Nicolas, K. E. Gubbins, W. B. Streett, and D. J. Tildesley, *Mol. Phys.*, **37**, 1429 (1979).
13. P. J. Steinbach and B. R. Brooks, *J. Comp. Chem.*, **15**, 667 (1994).
14. K. Tasaki, S. McDonald, and J. W. Brady, *J. Comp. Chem.*, **14**, 278 (1993).
15. J. Guenot and P. A. Kollman, *J. Comp. Chem.*, **14**, 295 (1993).
16. H. Schreiber and O. Steinhauser, *Chem. Phys.*, **168**, 75 (1992).
17. R. J. Loncharich and B. R. Brooks, *Proteins*, **6**, 32 (1989).
18. C. L. Brooks III, *J. Chem. Phys.*, **86**, 5156 (1987).
19. C. L. Brooks III, B. M. Pettitt, and M. Karplus, *J. Chem. Phys.*, **83**, 5897 (1985).
20. M. L. C. E. Kouwijzer, B. P. van Eijck, S. J. Kroes, and J. Kroon, *J. Comp. Chem.*, **14**, 1281 (1993).
21. R. R. Gabdoulline and Z. Zheng, *J. Comp. Chem.*, **16**, 1428 (1995).
22. G. Burley, *J. Chem. Phys.*, **38**, 2807 (1963).
23. S. C. Abrahams and J. L. Bernstein, *J. Chem. Phys.*, **55**, 3206 (1971).
24. N. Ishizawa and T. Miyata, *Acta Cryatallogr., Sect. B*, **36**, 228 (1980).
25. H. van Koningsveld, *Acta Crystallogr., Sect. B*, **43**, 127 (1987).
26. (a) for T, O, Na^1, and Na^3 sites: A, N. Fitch, H. Jobic, and A. Renouprez, *J. Phys. Chem.*, **90**, 1311 (1986); (b) for Na^4 site: A. G. Bezus, A. V. Kiselev, A. A. Lopatkin, and P. Q. Du, *J. Chem. Soc. Faraday Trans. II*, **74**, 367 (1978).
27. N. Karasawa and W. A. Goddard III, *J. Phys. Chem.*, **93**, 7320 (1989).
28. W. Loewenstein, *Am. Miner.*, **39**, 92 (1954).
29. C. Kittel, *Introduction to Solid State Physics*, 6th ed., Wiley, New York, 1980.
30. M. Abramowitz and I. A. Stegun, Eds., *Pocketbook of Mathematical Functions*, Verlag Harri Deutsch, Frankfurt am Main, Germany, 1984.
31. *Mathematica 2.2*, Wolfram Research, Inc., Champaign, IL, 1993.